ELSEVIER

Materials Science and Engineering B59 (1999) 319–322

MATERIALS SCIENCE & ENGINEERING B

Microcalorimetric absorption spectroscopy in GaN–AlGaN quantum wells

Axel Göldner [a,*], Axel Hoffmann [a], Bernard Gil [b], Pierre Lefebvre [b], Pierre Bigenwald [c], Philippe Christol [c], Hadis Morkoç [d]

[a] *Institut für Festkörperphysik, Technische Universität Berlin, Hardenbergstraße. 36, 10623 Berlin, Germany*
[b] *Groupe d'Etude des Semiconducteurs, CC074, Université de Montpellier II, Place Eugene Bataillon, Montpellier 34095, France*
[c] *Université d'Avignon et des Pays de Vaucluse, Boulevard Pasteur, 84000 Avignon, France*
[d] *Virginia Commonwealth University. 921 West Franklin Street. P.O. Box 843072, Richmond, VA 23284-3072, USA*

Abstract

Microcalorimetric measurements of small absorption coefficients have been performed on thin GaN–AlGaN quantum wells grown by Reactive Molecular Beam Epitaxy on Al_2O_3 substrates. In addition to strong absorption at the energy of the GaN buffer and at the energy of the thick AlGaN barrier layers, we could also readily detect transitions associated to the quantum well. These measurements which pave the way to a precise determination of the gap mismatch between the well and the barrier layers are combined with self consistent excitonic and envelope function calculations in the context of a model for the band line-ups which includes the piezoelectric effect. © 1999 Elsevier Science S.A. All rights reserved.

Keywords: Wide bandgap semiconductors; Low dimensional systems; Optical properties; Excitons

1. Experimental results

The sample investigated here was grown by Reactive Molecular Beam Epitaxy on a sapphire substrate, starting with three buffer layers of AlN (20 nm), GaN (1500 nm), $Ga_{0.93}Al_{0.07}N$ (100 nm), followed by a multiple quantum well (MQW) with five periods of 2.5 nm wide GaN confining layers, separated by 10 nm wide $Ga_{0.93}Al_{0.07}N$ barriers. The structure is capped by a $Ga_{0.93}Al_{0.07}N$ layer (40 nm). For the photo-thermal experiments on the GaAlN-MQW structures, we used the highly sensitive calorimetric absorption spectroscopy (CAS), calorimetric transmission spectroscopy (CTS) and calorimetric reflection spectroscopy (CRS) techniques at 47 mK [1]. In the CAS experiment, we measure the temperature increase of the photo-excited sample as function of the excitation energy. It is affected by the generation of phonons during nonradiative relaxation to thermal equilibrium. In CRS (CTS) experiments, the reflection (transmission) is detected by the absorption-induced heating of a black body.

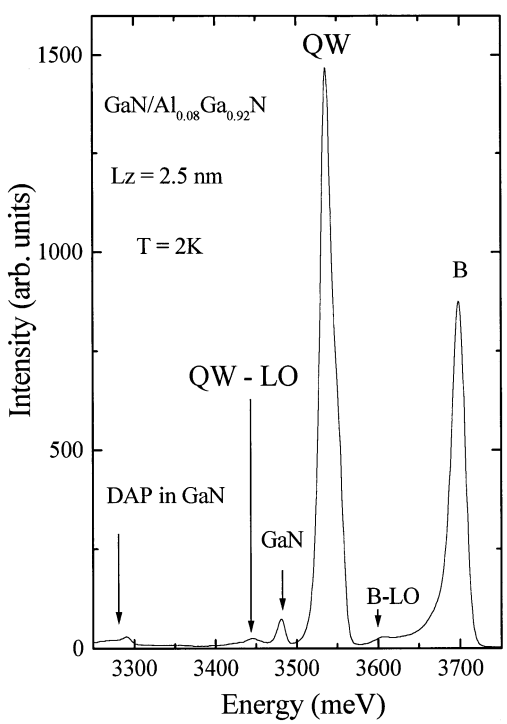

Fig. 1. 2K photoluminescence spectrum of the GaN–AlGaN MQW.

* Corresponding author.

0921-5107/99/$ - see front matter © 1999 Elsevier Science S.A. All rights reserved.
PII: S0921-5107(98)00363-8

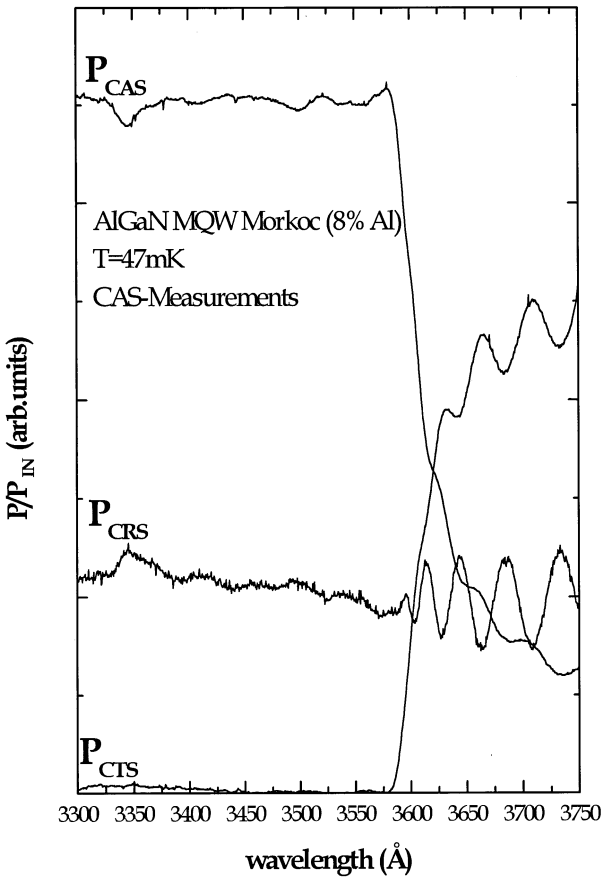

Fig. 2. Typical microcalorimetry spectra taken at 47 mK. Spectra correspond to micro calorimetric absorption, reflection, and transmission, respectively.

Fig. 1 represents a typical 2K photoluminescence spectrum taken using the 325 nm radiation of a HeCd laser. From high to low energies, one detects recombination in the barrier layer, its LO phonon replica, a signature of confined states, the photoluminescence of the GaN buffer layer, and the LO phonon replica of the quantum well confined state [2].

To quantify the contribution of nonradiative processes to the recombination mechanisms near the band edge, we employed calorimetric spectroscopy. Fig. 2 gives a set of simultaneously recorded high-resolution CAS, CTS, and CRS spectra. Three structures are clearly resolved in the CAS spectrum, (i) on the high energy side of the barrier luminescence at photon energies of 3.73 eV, a resonance line occurs which is typical for localised excitons in a disordered alloy, and which shows a typical Stokes shift. (ii) The resonance at 3.573 eV is attributed to transition energies of the fundamental heavy hole and light hole states of the GaAlN MQW structure. (iii) At photon energies of 3.520 eV the transition of localised excitons induced by well width and depth fluctuations can be detected. Additionally, the exciton transition of the GaN buffer layer can be observed at 3.483 eV. To obtain more explicit information from the CAS and the CRS spectra, both are shown in detail in Fig. 3. In addition to Fig. 2, one can see Fabry–Perot interferences in the lower energy range of the barrier luminescence. Thus, the dip in the CAS spectrum of the barrier luminescence mainly derives from the cap layer.

The decrease of the CAS signal at the spectral position of the above described transitions implies a decrease of the phonon emission rate and, therefore, enhanced radiative recombination. The evaluation of CTS, CRS, and CAS spectra shows that in this sample the quantum efficiencies are below 20% in the regarded examined spectral range. The barrier luminescence has a quantum efficiency of 7%, the resonance at 3.573 eV has a quantum efficiency of 11%, and the transitions associated with of the localised excitons have a quantum efficiency of 12%. These values reflects the macroscopic quantum efficiency, i.e. the rate of radiative relaxation which can leave the crystal.

2. Numerical calculations of the electronic structure

The eigenstates of the quantum structure are built from Bloch states of the binary and ternary materials convoluted with envelope functions. The decoupled electrons and heavy (Γ_9) hole states (labelled hh_i hereafter) are then calculated within the context of the one

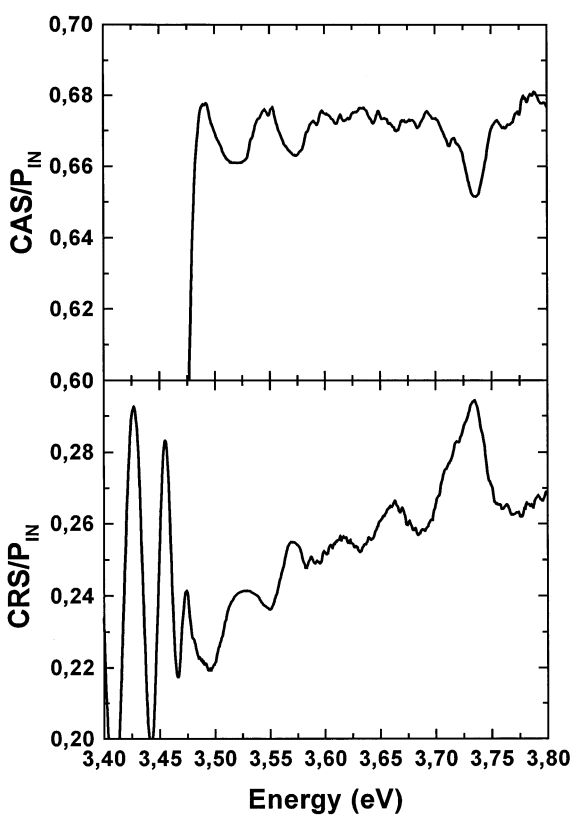

Fig. 3. High resolution plot of the CAS and the CRS spectra.

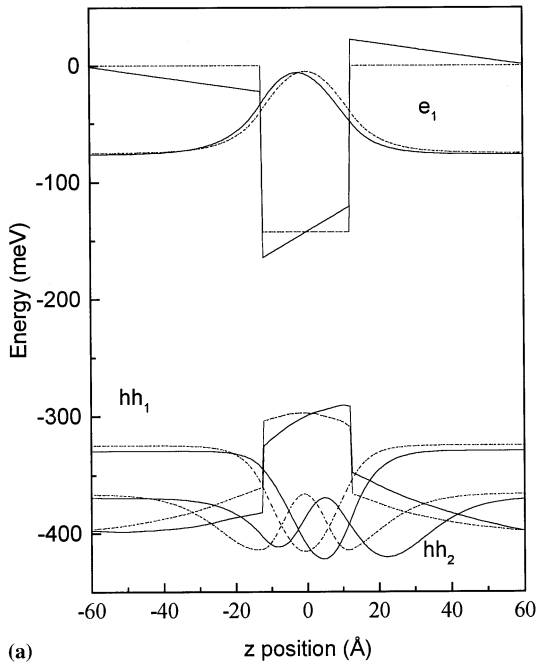

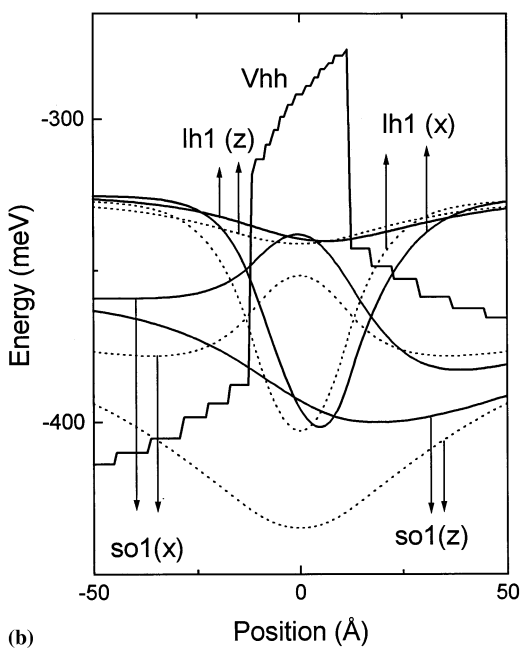

Fig. 4. (a) Typical electron (top of the figure), and heavy-hole (bottom of the figure), envelope functions computed in the absence (dotted line), and in the presence of the piezoelectric field. (b) Projections of the light hole and spin-orbit split-off hole envelope functions along Z and X like Bloch states. The calculation is made self-consistently without (dashed lines), and with (full line), piezoelectric field.

band envelope function approach since we place ourselves at $k_{\|}=0$. For these particles, the global wave functions are: $\Psi_e(1/2)=F_e|1/2\pm1/2\rangle$ and $\Psi_{hh}|\pm3/2=\Gamma_{hh}|3/2,\pm3/2\rangle$ where the Bloch functions $|1/2,\pm1/2\rangle$ and $|3/2,\pm3/2\rangle$ are $S(\uparrow)$, and $\mp1/\sqrt{2}|[X-(\pm)iY](\downarrow)\rangle$, respectively. As usual, S represents an s-like function in real space while X, Y, and latter Z are three p-like functions. The light-hole (lh_i) and spin-orbit split-off hole (so_i) states transform both like Γ_7 and a two-band envelope function calculation is required to find the eigenstates of the structure. In the spherical space, in terms of the projections of the angular momenta, we take:

$$|3/2,\pm1/2\rangle=2/\sqrt{6}|Z(\uparrow)\rangle\mp1/\sqrt{6}|[X\pm iY](\uparrow)\rangle$$

$$|1/2,\pm1/2\rangle=\pm1/\sqrt{3}|Z(\uparrow)\rangle+1/\sqrt{3}|[X\pm IY](\uparrow)\rangle$$

In the representation the good quantum numbers are the components of the total hole angular momentum, the corresponding wave functions are written as follows:

$$\Psi_{\Gamma7}(\pm1/2)=\phi_{lh}|3/2\pm1/2\rangle+\phi_{so}|1/2\pm1/2\rangle$$

which we first rearrange into:

$$\Psi_{\Gamma7}(\pm1/2)=\Phi_1|[X(\pm)iY](\uparrow)\rangle+\Phi_2|Z(\uparrow)\rangle$$

with

$$\Phi_1=-1/\sqrt{6}\phi_{lh}+1/\sqrt{3}\phi_{so}\quad\text{and}$$

$$\Phi_2=2/\sqrt{6}\phi_{lh}-1/\sqrt{3}\phi_{SO}$$

Neither of these two expansions is more appropriate than the other for computing the two-component envelope functions, physics does not have coordinates and changing the representation just changes the form of the extra-diagonal terms of the Hamiltonian for the kinetic energy in the valence band. A last expansion may be:

$$\Psi_{\Gamma7}(\pm1/2)=F_x|X(\downarrow)\rangle(\pm)iF_y|Y(\downarrow)\rangle+F_{so}|Z(\downarrow)\rangle$$

The potential depths are obtained from the position of the GaN bandgap measured by reflectance on the one hand and from the position of the bandgap of the alloy layer obtained either from the reflectance or from CAS, on the other. The depth of the conduction, heavy hole, light hole and spin orbit split-off hole line-ups are 171, 43.4, 42.5, and 22.8 meV, respectively [3]. The corresponding energies of the band to band transitions are, respectively, 3610, 3622, and 3656 meV. Both heavy and light hole states are well confined in the well layer whereas the split-off state, almost unconfined, is nearly degenerate with that of the AlGaN layers. For this reason, we have decided to correct our calculation by including the effect of the confined electrons on the valence potential through a self-consistent process with the exciton described previously in [4]. The exciton trial function has two variational parameters and the correction is made on the valence potential profile. The overlap integral between the electron envelope function and the X-related contribution the three electron-hole envelope integrals $|\langle\Psi_e|\Psi_h\rangle|^2$ are 49.6, 46.5 and 1.2%.

The binding energies are 50, 48, and 38 meV for A, B and C excitons with energies at 3561, 3574, and 3618 meV, respectively. Although the square well calculation

does not predict a confined hh_3 state the self-consistent calculation locates the e_1hh_3 excitonic at 3626 meV. The self-consistent hole wavefunction has two nodes, as expected. This makes the exciton binding energy to become smaller than in the bulk, 22.3 meV. The variational parameter is $\alpha = 0.5$ and the Bohr radius is $\lambda = 48$ Å. The values of the (α, λ) couples are (0.07, 30Å) for A(e_1-hh_1) and B(e_1-lh_1) and (0.25, 35Å) for C(e_1-so_1).

Now we can argue for the presence of piezoelectric fields through the sample. They have been included. A 200 kV cm^{-1} value was taken for the GaN layer [5], which was counterbalanced by an opposite field in the barrier layer so that there is no potential drop through the whole entire MQW system [6]. At the top of Fig. 4(a) are plotted the densities of probability for the electron in the absence (dotted line) and presence of piezoelectric field (full line) together with the conduction band line-up for a basic building block of the structure. The electron density of state is slightly distorted towards the left hand part of the figure. At the bottom of the figure the heavy-hole band line-ups are plotted (corrected from self-consistent long range Coulomb contribution produced by the electron-hole dipole) in both situations where the electric field is not included and is included (dotted lines, and full lines, respectively). We note that the maximum of the density of probability for hh_1 is displaced towards the right hand part of the figure.

We also point out that the distortion of hh_2 envelope function is significant. In Fig. 4(b) the projections of the lh_1 and so_1 probability densities of along the x and z components of the valence Bloch waves are shown. In terms of energies the quantum confined Stark effect brings the e_1hh_1, e_1lh_1, and e_1so_1 excitonic transitions to 3558.6, 3570.8, and 3594.6 meV, respectively. Thus there is a small red-shift with respect to the previous case (3561, 3574, and 3618 meV respectively). In terms of overlap, the values are 42.3, 40.8, and 2%, respectively. We note that we compute a transition at an energy of 3594.6 meV, which corresponds to a value of 1.37% for the overlap integral with the electron envelope function. The hole envelope function has one node, and consequently, the labelling is e_1hh_2. These calculations indicate that the weak structures hardly observed by CAS in the 3.6 eV region are of mixed nature, involve a spin-orbit split off confined state, and a second heavy hole confined level. The red-shift produced by the quantum confined Stark effect due to the influence of the built-in piezoelectric field remains small because these quantum wells are very thin.

3. Conclusion

We have reported the first investigation of the optical properties of GaN–GaAlN quantum wells by microcalorimetry. The experiment delivered the values of the quantum efficiency. A sophisticated envelope function calculation has led us to the values of the exciton binding energies and oscillator strengths. The calculations indicate that the effect of the built-in piezoelectric field is moderate in these MQWs. This we find to be consistent with a balancing distribution of this piezoelectric field in the barrier layers, in close agreement with the situation in GaInAs–GaAs MQWs [7]. This study offers us the possibility to anticipate besides the gain in oscillator strengths the optical confinement, in line with the number of quantum wells. The thresholds for lasing in nitride-based MQWs are probably lowered by this distribution of piezoelectric field in the barrier layers. Such a distribution counterbalances the quantum confined Stark effect in single quantum wells.

Acknowledgements

This work was partly made under the context of a French–German PROCOPE contract under number 98134.

References

[1] L. Podlowski, A. Hoffmann, I. Broser, J. Cryst. Growth 177 (1992) 698.
[2] P. Lefebvre, J. Allegre, B. Gil, et al., Phys. Rev. B 57 (1998) 9447.
[3] M. Suzuki, T. Uenoyama, in: B. Gil (Ed.), Group III Nitride Semiconductor Compounds, Clarendon Press, Oxford, 1998.
[4] B. Gil, P. Bigenwald, Solid State Commun. 94 (1995) 883.
[5] J.S. Im, J. Off, A. Sohmer, F. Scholz, A. Hangleiter, Mater. Sci. Forum 264-268 (1998) 1299.
[6] D.L. Smith, C. Mailhiot, Rev. Mod. Phys. 62 (1990) 173.
[7] B. Laurich, K. Elcess, C.G. Fonstad, J.G. Beery, C. Mailhiot, D.L. Smith, Phys. Rev. Lett. 62 (1989) 649.